

Synthesis, Molecular Structure and Antioxidant Activity of (*E*)-4-[Benzylideneamino]-1,5-dimethyl-2-phenyl-1*H*-pyrazol-3(2*H*)-one, a Schiff Base Ligand of 4-Aminoantipyrine

Mohammad Sayed Alam · Dong-Ung Lee

Received: 9 March 2011 / Accepted: 17 November 2011 / Published online: 18 December 2011
© Springer Science+Business Media, LLC 2011

Abstract In this study, the title compound, C₁₈H₁₇N₃O ($M_r = 291.35$), was synthesized by the condensation reaction of 4-amino-1,5-dimethyl-2-phenylpyrazole-3-one and benzaldehyde. Single-crystal X-ray diffraction data revealed that this compound adopts a *trans* configuration around the central C=N double bond. It crystallizes in the monoclinic, space group $P2_1/c$ with $a = 12.9236(17)$ Å, $b = 6.8349(9)$ Å, $c = 17.072(2)$ Å, $\beta = 90.316(3)^\circ$, $V = 1508.0(3)$ Å³, $Z = 4$, $D_c = 1.283$ Mg/m³, $F(000) = 616$, $\mu = 0.082$ mm⁻¹, $R = 0.0442$, and $wR = 0.0936$. Two different planes exist within the molecule; e.g. the pyrazolone and benzylidene groups attached to C9 of the pyrazolone ring are almost coplanar, whereas the phenyl group attached to the N1 of the pyrazolone ring is in another plane. Density functional theory (DFT) and time-dependent DFT calculations were performed to predict the electronic structure and absorption spectra of (*E*)-4-[benzylideneamino]-1,5-dimethyl-2-phenyl-1*H*-pyrazol-3(2*H*)-one, a schiff base ligand of 4-aminoantipyrine using B3LYP/6-311G basis set on the AM1 optimized geometry. The predicted vibrational frequencies using the B3LYP/6-311G method were in strong agreement with the experimental IR spectra. The time dependent DFT calculations were used to evaluate the electronic absorption spectrum and three electron transition bands, which were mainly derived from the

contribution of $n \rightarrow \pi^*$ and $\pi \rightarrow \pi^*$ transitions, were observed in both the experimental and predicted UV–Vis spectra. A maximum emission band at 370 nm was observed in the fluorescence spectra of the title compound. In addition, the title compound showed good DPPH antioxidant activity.

Keywords Pyrazole-3-ones · Crystal structure · Density functional theory · Quantum chemical calculation

Introduction

In the last few decades, Schiff base compounds have received much attention in the field of chemistry and biology due to their chemotherapeutic value [1–3]. Schiff base compounds have also been used as effective ligands for metal ions in the preparation of dyes, liquid crystals and powerful corrosion inhibitors. 4-Amino-1,5-dimethyl-2-phenylpyrazole-3-one (4-aminoantipyrine) forms a variety of Schiff bases with aldehydes and their transition metal complexes showed a wide range of biological activities and applications [4–6].

Free radicals including reactive oxygen species (ROS) cause oxidative stress in biological systems. Antioxidants have been shown to play an important role in protecting humans against many fatal diseases. Antioxidants have been widely used in medicine and different fields of industry to interrupt radical-chain oxidation processes, improve general health, help cell rejuvenation and prevent cancer [7]. Quantum-chemical parameters have been used to help describe the properties of antioxidant substances in detail. Density functional theory (DFT) has received much interest as a reliable standard tool for the quantum chemical calculation of molecular structures and biological

M. S. Alam (✉) · D.-U. Lee (✉)
Division of Bioscience, Dongguk University, Gyeongju 780-714,
Republic of Korea
e-mail: alam_sms@dongguk.ac.kr; alam_sms@yahoo.com

D.-U. Lee
e-mail: dulee@dongguk.ac.kr

M. S. Alam
Department of Chemistry, Jagannath University,
Dhaka 1100, Bangladesh

properties of molecule. In recent years, DFT has been extensively used to study the structures and absorption spectra of different classes of compounds [8–11]. DFT studies can provide useful information in regards to the coordination properties of ligands. A remarkable number of Schiff base ligands of 4-aminoantipyrine have recently been reported [12–17] but their quantum chemistry calculation have not yet been studied. In the present study, we report the molecular structure, spectral properties and antioxidant activity of (*E*)-4-[benzylideneamino]-1,5-dimethyl-2-phenyl-1*H*-pyrazol-3(2*H*)-one, a Schiff base derivative of 4-aminoantipyrine, which will provide useful information to explain the coordination properties of the Schiff bases of aminoantipyrine.

Experimental Section

General

The melting point was determined using a Stuart SMP3 apparatus and was uncorrected. The ^1H and ^{13}C NMR spectra were recorded using TMS as a reference standard in CDCl_3 solvent on a Varian GEMINI 200 spectrophotometer. FT-IR spectra, as KBr pellets, were obtained using a Bruker Tensor 37 spectrophotometer. Electronic absorption spectra were measured on a Varian Cary 4000 spectrophotometer in an EtOH solution and fluorescence spectra were measured on Varian Cary Eclipse Fluorescence spectrophotometer. FAB-MS spectra were acquired using a Jeol JMS-700 mass spectrometer. Crystal data collection: Bruker SMART; cell refinement: Bruker SAINT; data reduction: Bruker SAINT; program(s) used to solve structure: Bruker SHELXTL; program(s) used to refine the structure: Bruker SHELXTL; molecular graphics: Bruker SHELXTL. Absorbance for antioxidant activity was measured on Optizen 2120 UV/VIS Spectrophotometer (Mecasys Co. Ltd., Korea).

Synthesis and Crystallization

An anhydrous ethanol solution (10 mL) of 4-amino-1,5-dimethyl-2-phenylpyrazol-3-one (203 mg, 1 mmol) was added to an anhydrous ethanol solution (10 mL) of benzaldehyde (106 mg, 1 mmol) and the mixture was refluxed at 80 °C for 4 h under atmospheric conditions (Scheme 1). The precipitate formed was collected by filtration and purified by recrystallization from ethanol, and then dried in vacuo to

give the pure compound with a yield of 85%, m.p. 178.3 °C. Single yellow crystals of the title compound suitable for X-ray analysis were obtained by slow evaporation of an ethanol solution. The constitution of 4-[benzylideneamino]-1,5-dimethyl-2-phenyl-1*H*-pyrazol-3(2*H*)-one was supported by ^1H NMR, ^{13}C NMR, IR and HRMS analysis.

^1H NMR (200 MHz, CDCl_3): δ 2.49 (s, 3H, =C–CH₃), 3.14 (s, 3H, –N–CH₃), 7.31–7.52 (m, 8H, ArH), 7.84–7.89 (m, 2H, ArH), 9.77 (s, 1H, –N=CH). ^{13}C NMR (62.5 MHz, CDCl_3): δ 10.91, 35.83, 110.30, 125.15, 129.60, 127.51, 128.00, 128.70, 130.32, 134.90, 138.11, 150.30, 160.79, 163.38. HRMS-FAB (m/z): $[\text{M} + \text{H}]^+$ calculated for $\text{C}_{18}\text{H}_{17}\text{N}_3\text{O}$, 292.1338; found 292.1339 (error: +0.4 ppm).

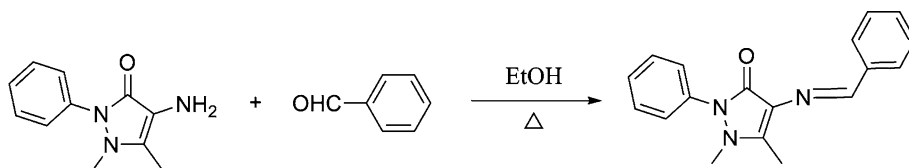
Crystal Structure Determination

The solvent loss technique was used to grow yellow plate-shaped crystals of the title compound. A single crystal of suitable size (0.29 mm \times 0.16 mm \times 0.07 mm) was chosen for the X-ray diffraction studies. The data were collected at a temperature of 200(2) K on a Bruker SMART CCD area detector diffractometer [18] with graphite monochromated radiation $\text{MoK}\alpha$ ($\lambda = 0.71073$ Å). A total of 20,373 reflections were collected, of which 3,758 ($-17 \leq h \leq 17$, $-9 \leq k \leq 9$, $-22 \leq l \leq 22$) were treated as observed. The structure was solved by direct methods using SHELXTL [19, 20]. Full-matrix least-squares refinement using SHELXTL with isotropic displacement parameters for all the non hydrogen atoms converged the residual to $R_1 = 0.1676$. Subsequent refinements [21] were carried out with anisotropic thermal parameters for the non-hydrogen atoms. The hydrogen atoms were fixed at chemically acceptable positions and were allowed to ride on their parent atoms, with a C–H distance of 0.9500–0.9800 Å. The final refinement converged to $R = 0.0442$, $wR = 0.0936$, $w = 1/[s^2(F_o)^2 + (0.0633P)^2 + 0.00P]$, where $P = (F_o^2 + 2F_c^2)/3$, $S = 0.755$, $(\Delta/\sigma)_{\text{max}} < 0.001$, $(\Delta\rho)_{\text{max}} = 0.207$ and $(\Delta\rho)_{\text{min}} = -0.262 \text{ e Å}^{-3}$.

Quantum Chemical Calculations

The molecular geometries of the title compound were optimized using MM+ molecular modeling and semi-empirical molecular orbital AM1 methods [22]. The DFT calculations with a hybrid functional B3LYP (Becke's three parameter nonlocal exchange functional along with

Scheme 1 Synthesis of (*E*)-4-[benzylideneamino]-1,5-dimethyl-2-phenyl-1*H*-pyrazol-3(2*H*)-one



the Lee–Yang–Parr correlation functional) [23, 24] at basis set 6-311G were then performed using the GAMESS (version March 25, 2010 R2) software package [25]. No imaginary frequencies were obtained in the vibrational frequencies calculations indicating that the structures were stable. After optimization, Mulliken charge and properties of frontier molecular orbitals (FMOs) of the title compound were analyzed using the results calculated at the B3LYP/6-311G level.

DPPH Radical Scavenging Activity

The free radical-scavenging activity of the title compound was assayed according to the Blois method with some modification [26] using 1,1-diphenyl-2-picrylhydrazyl (DPPH). 0.1 mL of different concentrations (2.5–20 mg/mL) of sample in ethanol were added to 4 mL of a 1.5×10^{-5} M DPPH solution and mixed thoroughly. The solution was then left to stand at room temperature in the dark. After 30 min of incubation, the absorbance of the solution was measured at 520 nm and the antioxidant activity was calculated using the following equation:

$$\text{DPPH radical-scavenging activity \%} = \left[\frac{(\text{Absorbance of the control} - \text{Absorbance of the sample})}{\text{Absorbance of the control}} \right] \times 100$$

Results and Discussion

Synthesis and Structural Description

The title compound was synthesized in good yield using a condensation reaction of 4-amino-1,5-dimethyl-2-phenylpyrazole-3-one with benzaldehyde as shown in Scheme 1. The chemical structure of the synthesized compound was confirmed by spectroscopic methods, and the exact stereochemistry was determined by X-ray crystal analysis.

Details of the X-ray diffraction crystal data and structure refinement for the title compound are shown in Table 1. The title compound crystallized in the monoclinic, space group $P2_1/c$ with $a = 12.9236(17)$ Å, $b = 6.8349(9)$ Å, $c = 17.072(2)$ Å, $\beta = 90.316(3)^\circ$, $V = 1508.0(3)$ Å³, $Z = 4$, $D_c = 1.283$ Mg/m³, $F(000) = 616$, $\mu = 0.082$ mm^{−1}, $R = 0.0442$, and $wR = 0.0936$. Bond lengths and angles of all the non-hydrogen atoms of 4-[benzylideneamino]-1,5-dimethyl-2-phenyl-1*H*-pyrazol-3(2*H*)-one (Table 2) were within normal ranges [27]. The ORTEP diagram of the molecule is shown in Fig. 1a, with thermal ellipsoids drawn at a 50% probability. The geometry was calculated using software (Bruker SHELXTL). As shown in Fig. 1a, the pyrazolone ring (C8–C10/N1/N2/N3/O1) was almost

Table 1 Crystal data and structure refinement for (*E*)-4-[benzylideneamino]-1,5-dimethyl-2-phenyl-1*H*-pyrazol-3(2*H*)-one

| | |
|---|--|
| Empirical formula | C ₁₈ H ₁₇ N ₃ O |
| Formula weight | 291.35 |
| Temperature | 200(2) K |
| Wavelength | 0.71073 Å |
| Crystal system | Monoclinic |
| Space group | $P2_1/c$ |
| Hall symbol | − <i>P</i> 2ybc |
| Unit cell dimensions | $a = 12.9236(17)$ Å $b = 6.8349(9)$ Å $c = 17.072(2)$ Å $\beta = 90.316(3)^\circ$ |
| Volume | 1508.0(3) Å ³ |
| <i>Z</i> | 4 |
| Density (calculated) | 1.283 Mg/m ³ |
| Absorption coefficient | 0.082 mm ^{−1} |
| <i>F</i> (000) | 616 |
| Crystal size | 0.29 × 0.16 × 0.07 mm ³ |
| Theta range for data collection | 1.58 to 28.34° |
| Index ranges | −17 ≤ <i>h</i> ≤ 17, −9 ≤ <i>k</i> ≤ 9, −22 ≤ <i>l</i> ≤ 22 |
| Reflections collected | 20,373 |
| Independent reflections | 3758 [<i>R</i> (int) = 0.1319] |
| Completeness to theta = 28.34° | 99.9% |
| Absorption correction | None |
| Refinement method | Full-matrix least-squares on <i>F</i> ² |
| Data/restraints/parameters | 3758/0/201 |
| Goodness-of-fit on <i>F</i> ² | 0.755 |
| Final <i>R</i> indices [<i>I</i> > 2σ(<i>I</i>)] | <i>R</i> ₁ = 0.0442, <i>wR</i> ₂ = 0.0936 |
| <i>R</i> indices (all data) | <i>R</i> ₁ = 0.1602, <i>wR</i> ₂ = 0.1626 |
| Largest diff. peak and hole | 0.207 and −0.262 e Å ^{−3} |

planar, with an r.m.s. deviation for fitted atoms of 0.0337 Å, and a dihedral angle of 67.04° with its attached phenyl ring (C1–C6). Torsion angles of N2–N1–C1–C6 and N2–N1–C1–C2 were −150.7(2) and 32.6(5)°, respectively. The atom O1 only slightly deviated from the pyrazolone mean plane, with torsion angles value of C10–C9–C8–O1 and N2–N1–C8–O1 are 175.2(3) and −171.0(2)°, respectively. The C7 and C11 atoms were located on the opposite side of the pyrazolone plane and the torsion angle of C11–C10–N2–C7 was −24.3(4)°. Due to conjugation through the imino double bond C12=N3, the pyrazolone and the C13–C18 phenyl were approximately coplanar, with a dihedral angle between them of 3.9°. The torsion angles value of C10–C9–N3–C12, C8–C9–N3–C12, C13–C12–N3–C9, C14–C13–C12–N3 and C18–C13–C12–N3 were −179.2(3), −8.7(4), 176.1(2), 2.9(4) and −176.7(3)°, respectively. The packing arrangement in the crystal structure of (*E*)-4-[benzylideneamino]-1,5-dimethyl-2-phenyl-1*H*-pyrazol-3(2*H*)-one are shown in Fig. 2, with intermolecular and

Table 2 Selected bond lengths (Å) and angles (°) by X-ray and theoretical calculations for (*E*)-4-[benzylideneamino]-1,5-dimethyl-2-phenyl-1*H*-pyrazol-3(2*H*)-one at B3LYP/6-311G level of theory

| | Exp. | Calc. |
|-------------------------|----------|-------|
| Bond lengths (Å) | | |
| C(1)–C(6) | 1.382(4) | 1.406 |
| C(1)–C(2) | 1.384(4) | 1.405 |
| C(1)–N(1) | 1.420(3) | 1.441 |
| C(2)–C(3) | 1.389(4) | 1.397 |
| C(3)–C(4) | 1.378(4) | 1.395 |
| C(4)–C(5) | 1.379(4) | 1.397 |
| C(5)–C(6) | 1.378(4) | 1.393 |
| N(1)–N(2) | 1.405(3) | 1.441 |
| N(1)–C(8) | 1.406(3) | 1.426 |
| N(2)–C(10) | 1.353(3) | 1.391 |
| N(2)–C(7) | 1.463(3) | 1.481 |
| C(8)–O(1) | 1.237(3) | 1.255 |
| C(8)–C(9) | 1.436(4) | 1.455 |
| C(9)–C(10) | 1.369(4) | 1.372 |
| C(9)–N(3) | 1.394(3) | 1.395 |
| C(10)–C(11) | 1.485(4) | 1.490 |
| N(3)–C(12) | 1.285(3) | 1.299 |
| C(12)–C(13) | 1.469(4) | 1.464 |
| C(13)–C(18) | 1.382(4) | 1.407 |
| C(13)–C(14) | 1.393(4) | 1.408 |
| C(14)–C(15) | 1.376(4) | 1.393 |
| C(15)–C(16) | 1.373(4) | 1.402 |
| C(16)–C(17) | 1.372(4) | 1.398 |
| C(17)–C(18) | 1.392(4) | 1.395 |
| Bond angles (°) | | |
| C(6)–C(1)–C(2) | 120.6(3) | 118.7 |
| C(6)–C(1)–N(1) | 117.3(3) | 119.1 |
| C(2)–C(1)–N(1) | 122.0(3) | 122.1 |
| C(1)–C(2)–C(3) | 119.1(3) | 120.3 |
| C(4)–C(3)–C(2) | 120.2(3) | 120.8 |
| C(3)–C(4)–C(5) | 120.1(3) | 118.9 |
| C(6)–C(5)–C(4) | 120.2(3) | 121.0 |
| C(5)–C(6)–C(1) | 119.6(3) | 120.2 |
| N(2)–N(1)–C(8) | 108.7(2) | 107.9 |
| N(2)–N(1)–C(1) | 119.5(2) | 120.4 |
| C(8)–N(1)–C(1) | 122.1(2) | 124.2 |
| C(10)–N(2)–N(1) | 107.3(2) | 107.2 |
| C(10)–N(2)–C(7) | 126.0(2) | 121.2 |
| N(1)–N(2)–C(7) | 119.0(2) | 118.6 |
| O(1)–C(8)–N(1) | 123.0(3) | 124.6 |
| O(1)–C(8)–C(9) | 131.9(3) | 129.2 |
| N(1)–C(8)–C(9) | 105.0(2) | 106.2 |
| C(10)–C(9)–N(3) | 121.9(3) | 123.3 |
| C(10)–C(9)–C(8) | 107.9(2) | 108.1 |
| N(3)–C(9)–C(8) | 129.6(3) | 128.5 |
| N(2)–C(10)–C(9) | 110.4(3) | 110.6 |

Table 2 continued

| | Exp. | Calc. |
|-------------------|----------|-------|
| N(2)–C(10)–C(11) | 122.0(3) | 121.6 |
| C(9)–C(10)–C(11) | 127.6(3) | 127.7 |
| C(12)–N(3)–C(9) | 121.6(2) | 121.4 |
| N(3)–C(12)–C(13) | 120.6(3) | 121.6 |
| C(18)–C(13)–C(14) | 118.9(3) | 119.0 |
| C(18)–C(13)–C(12) | 119.9(3) | 118.3 |
| C(14)–C(13)–C(12) | 121.2(3) | 122.7 |
| C(15)–C(14)–C(13) | 120.4(3) | 120.3 |
| C(16)–C(15)–C(14) | 120.4(3) | 120.3 |
| C(17)–C(16)–C(15) | 119.8(3) | 119.9 |
| C(16)–C(17)–C(18) | 120.3(3) | 119.9 |
| C(13)–C(18)–C(17) | 120.1(3) | 120.6 |

intramolecular hydrogen bonding interactions. The hydrogen-bond geometry are shown in Table 3. Weak non-classical intermolecular C–H···O and C–H···N hydrogen bonds stabilized the crystal packing of title compound. An intramolecular C–H···O hydrogen-bonding interaction is also found, which helps to stabilize the conformation of the molecule.

DFT Calculations

The optimized geometric parameters obtained from the DFT-B3LYP/6-311G calculations of the title compound are listed in Table 2. The theoretical geometric structure of the molecule is shown in Fig. 1b. Comparisons between the experimental bond lengths and the calculated bond lengths indicated that all optimized bond lengths were slightly larger than the experimental values. This was the case because the experimental data was collected in the solid phase, whereas the calculated values corresponded to the isolated molecule in gas phase. The highest bond length difference was 0.038 Å for the N2–C10 bond, whereas the biggest bond angle deviation occurred in the C10–N2–C7 angle (4.8°). There are two probable reasons for the above discrepancies: the calculated data were for the molecule in a gas phase and no molecular interactions were considered, whereas the experimental data was acquired in the solid state and crystal field interactions were present. The geometry of the molecule in the solid state was subject to various intermolecular interactions, e.g. van der Waals forces, crystal packing forces and hydrogen-bond interactions [28]. Another reason for this discrepancy is that in the solid state, there exist intermolecular hydrogen bond interactions between N2 and H11 and steric hindrance between the two methyl groups attached to N2 and C10, while in the theoretical calculations, the interactions were neglected, which, to some extent, may have led to a higher bond angle of C10–N2–C7 in the solid state. Despite these

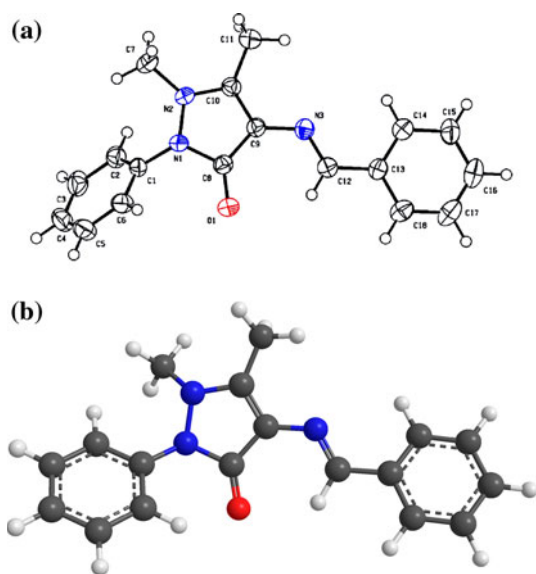


Fig. 1 **a** The molecular structure of (*E*)-4-[benzylideneamino]-1,5-dimethyl-2-phenyl-1*H*-pyrazol-3(2*H*)-one, showing 50% probability displacement ellipsoids and the atom-numbering scheme. **b** The theoretical geometric structure of (*E*)-4-[benzylideneamino]-1,5-dimethyl-2-phenyl-1*H*-pyrazol-3(2*H*)-one

some differences, the aforementioned comparisons suggest that the DFT-B3LYP/6-311G method [29] can produce satisfactory precision and reproduce the crystal structure of the title compound, which are the bases for our following discussion.

Fig. 2 Packing arrangement in the crystal structure of (*E*)-4-[benzylideneamino]-1,5-dimethyl-2-phenyl-1*H*-pyrazol-3(2*H*)-one. Dashed lines indicate hydrogen bonds

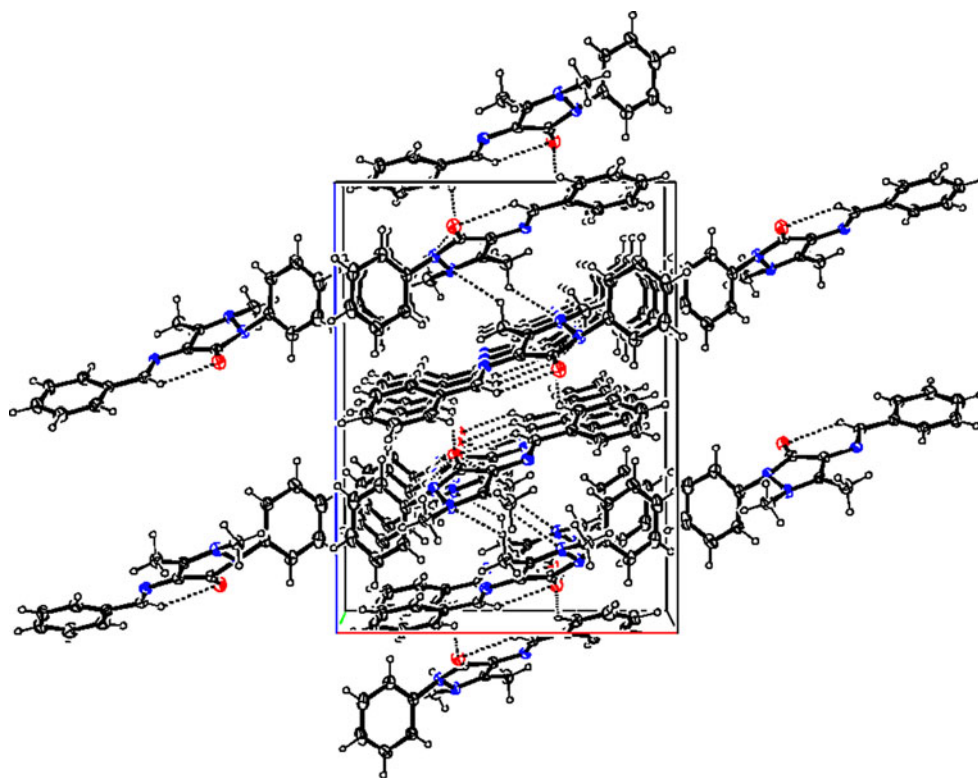


Table 3 Hydrogen-bond geometry (Å, °)

| D–H···A | D–H (Å) | H···A (Å) | D···A (Å) | D–H···A (°) |
|------------------------------|---------|-----------|-----------|-------------|
| C7–H7a···O1 ⁱ | 0.98 | 2.67 | 3.482 | 139.9 |
| C18–H18···O1 ⁱⁱ | 0.95 | 2.61 | 3.332 | 126.7 |
| C11–H11a···N2 ⁱⁱⁱ | 0.98 | 3.04 | 3.687 | 124.1 |

Symmetry codes: (i) $x, -y + 1/2, z - 3/2$; (ii) $-x + 1, y - 1/2, -z + 3/2$; (iii) $x, y - 1, z$

D donor atom, *H* hydrogen atom, *A* acceptor atom

Vibrational Frequencies

Figure 3 shows the comparison between the experimental and the virtual infrared spectra, where the calculated frequencies are plotted against intensity. The vibrational frequencies were predicted using the B3LYP/6-311G level of the theory at a spin multiplicity of one and the GAMESS (version March 25, 2010 R2) software package [25] was used to assign the calculated harmonic frequencies. Some primary calculated harmonic frequencies and their description concerning the assignment are listed in Table 4. According to the results presented in Table 4 and Fig. 3, the differences between the experimental and predicted frequencies were relatively small. Therefore, the DFT-B3LYP/6-311G method used in the present study can accurately predict the vibrational frequencies of the title compound.

Fig. 3 Experimental IR spectra (top) and simulated IR spectra at the B3LYP/6-311G level of the theory (bottom) for the title compound

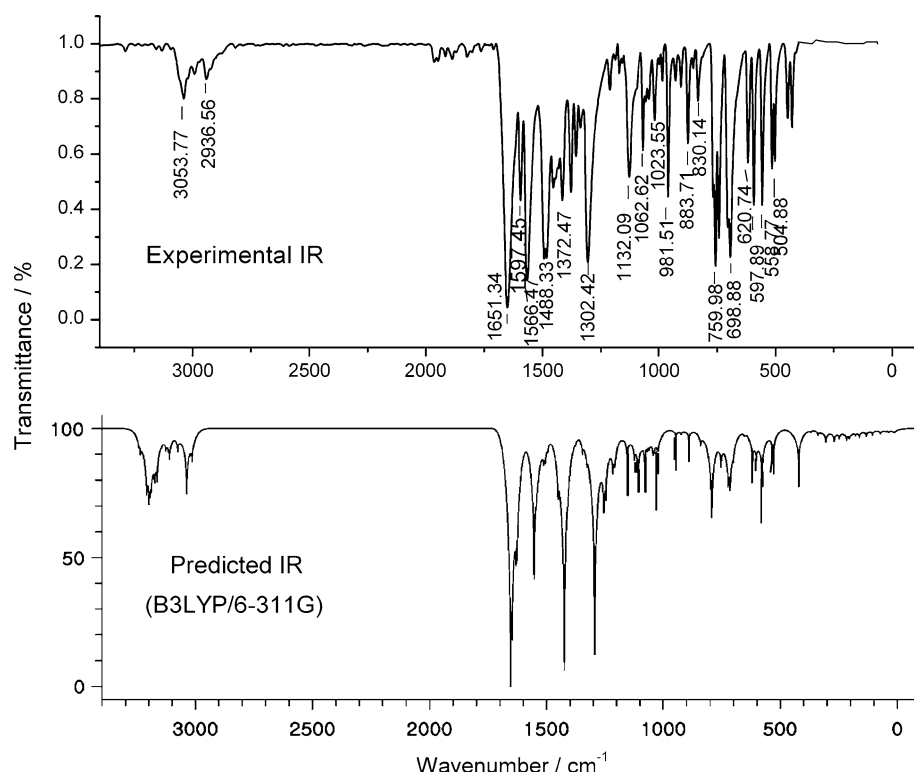


Table 4 Comparison of some experimental and calculated vibrational spectra of the title compound

| Assignments | Exp. | Calc. (B3LYP/ 6-311G) |
|--------------------------------------|-------------|-----------------------------|
| C–H str. in phenyl ring | 3,054 | 3,215–3,177 |
| C–H str. in methyl group | 2,937 | 3,045 |
| >C=O functional group | 1,651 | 1,666 |
| C=N str. and C–C def. in phenyl ring | 1,597–1,566 | 1,568–1,538 |
| C–H def. in phenyl ring | 1,488 | 1,457 |
| C–H def. in methyl group | 1,372 | 1,318 |
| C–O str. in carbonyl group | 1,302 | 1,248 |
| N–N str. and all C–H def. | 1,132 | 1,117 |
| N–N str. and all C–N str. | 1,062 | 1,046 |
| All of the C–H def. | 884 | 907 |
| Molecular skeleton def. | 830 | 853 |
| C–C def. in phenyl ring | 760 | 791 |
| C–H def. in phenyl ring | 698 | 721 |
| Molecular skeleton def. | 597 | 581 |

str stretching, def deformation

Energy of FMOs and Mulliken Charge Distribution

The FMOs play an important role in determining the reactivity and ability of a molecule to absorb light. These FMOs are important for the optical and electric properties and molecular reactivity. The single point energy and

FMOs were calculated according to the quantum chemical calculations and in the calculation, 35 atoms, which involved 337 basis functions including 77 occupied orbitals, were shown to be involved.

According to the molecular orbital theory, the HOMO–LUMO and the vicinal molecular orbitals are involved in the coordination property of a molecule and the molecular stability depends on the negative energy values of the FMOs [30]. The energy levels of the HOMO-2, HOMO-1, HOMO, LUMO+1 and LUMO+3 orbitals computed at the B3LYP/6-311G level for the title compound are shown in Fig. 4. The energy of HOMO and LUMO and the energy differences were -9.14 , -5.52 and 3.62 eV, respectively. The total energy (-1035 a.u.) of the title compound was lower and the energies of HOMO and LUMO and their neighboring orbitals were all negative, which indicates that the title compound was stable. The HOMO and its vicinal orbital play the role of electron donors, and the LUMO and its vicinal orbital play the role of electron acceptors.

Based on the optimized structure of the title compound, the Mulliken charge distribution of all atoms was calculated and the results are given in Table 5. This analysis indicated that the atomic electro negativity plays an important role in the Mulliken charge distribution. Namely, between the two connecting atoms, the atom having a higher electronegativity will carry negative charges, while the atom having a lower electronegativity will carry positive charges [28]. Thus, for the title compound, H and C

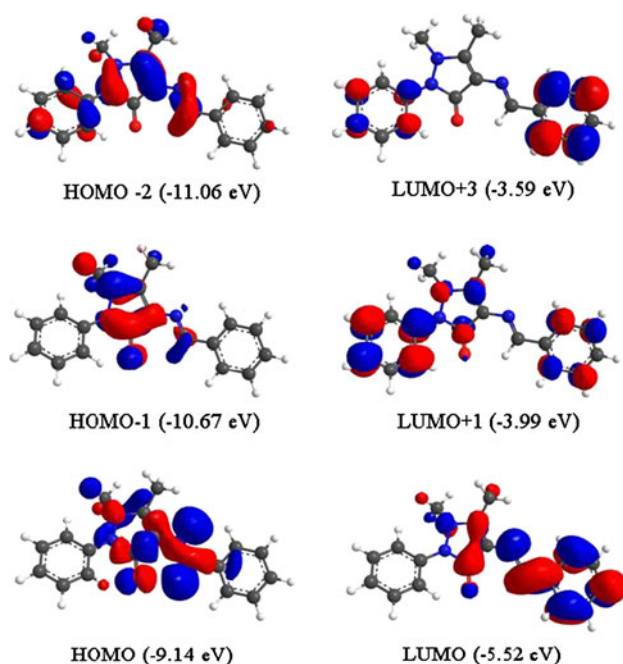


Fig. 4 Contour plots and energy of some frontier molecular orbitals in the title compound

(non-bonding with H atoms) were all positive, while N (from pyrrole ring and imine), O (bonding with C) and C (bonding with H) were all negative. Therefore, the hetero atoms, e.g. O1, N1, N2 and N3, bearing the negative charge could act as an electron donor when coordinating with metals except C7 and C11. According to the Mulliken charge distribution, these two atoms also have relatively large negative values and might not be involved in coordination with metals due to the steric hindrance between the C7 and C11 methyl groups. The crystal structure of the title compound also revealed that the two methyl groups were located opposite to the pyrazolone ring due to steric hindrance. The HOMO contour plot (Fig. 4) of the title compound shows that the electron density around the C7 and C11 atoms was much lower than O1, N1, N2 and N3 atoms, which resulted in a lack of electron donor capacity of the former two atoms.

UV-Absorption Spectra

Experimental electronic absorption spectra were measured in an ethanol solution at room temperature and theoretical electronic absorption spectra were predicted using the TD-DFT method based on the B3LYP/6-311G level optimized structure of the title compound. The calculated and experimental electronic spectrums are shown in Fig. 5. Table 6 represents the most important calculated electronic transition models of the title compound. As shown in Fig. 5 and Table 6, both the experimental and calculated data

Table 5 Mulliken charges (*e*) for the title compound

| Atom | Charge/ <i>e</i> |
|--------|------------------|
| O(1) | −0.437 |
| N(1) | −0.610 |
| N(2) | −0.400 |
| N(3) | −0.358 |
| C(1) | 0.284 |
| C(2) | −0.133 |
| C(3) | −0.174 |
| C(4) | −0.122 |
| C(5) | −0.169 |
| C(6) | −0.130 |
| C(7) | −0.394 |
| C(8) | 0.645 |
| C(9) | −0.203 |
| C(10) | 0.453 |
| C(11) | −0.584 |
| C(12) | −0.070 |
| C(13) | −0.060 |
| C(14) | −0.051 |
| C(15) | −0.175 |
| C(16) | −0.123 |
| C(17) | −0.167 |
| C(18) | −0.143 |
| H(2) | 0.173 |
| H(3) | 0.146 |
| H(4) | 0.153 |
| H(5) | 0.152 |
| H(6) | 0.224 |
| H(7A) | 0.203 |
| H(7B) | 0.221 |
| H(7C) | 0.218 |
| H(11A) | 0.238 |
| H(11B) | 0.203 |
| H(11C) | 0.207 |
| H(12) | 0.206 |
| H(14) | 0.167 |
| H(15) | 0.148 |
| H(16) | 0.150 |
| H(17) | 0.149 |
| H(18) | 0.164 |

showed the presence of three bands with some discrepancies. The difference between the experimental values and predicted values may be due to the following reasons: The TD-DFT approach is based on the random-phase approximation (RPA) method [31] and spin–orbit splitting is not considered in the calculation; the values are averaged. In our study, the electronic structure was evaluated by direct electronic excitations and only singlet–singlet transitions were considered. In addition, the role of the ethanol solvent

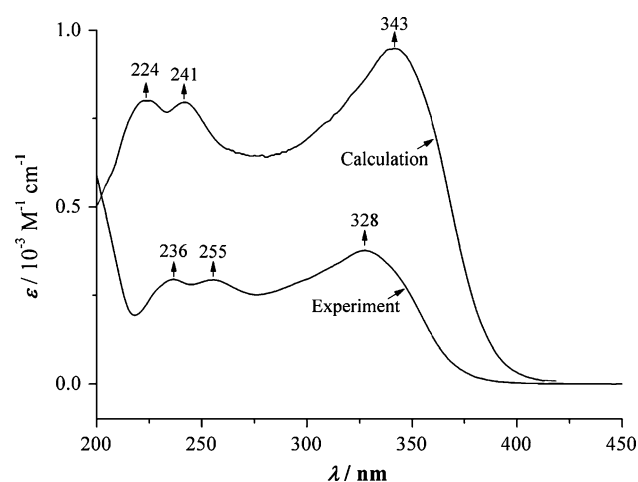


Fig. 5 Experimental and calculated electronic absorption spectra of the title compound

Table 6 Experimental and calculated electronic absorption spectra values

| Exp. | Calc. (TD-DFT) | | |
|------------------|------------------|---------------------|--------------------------------|
| Wave length (nm) | Wave length (nm) | Oscillator strength | Electronic transition |
| 236 | 224 | 0.2709 | HOMO → LUMO+3 HOMO-2 → LUMO |
| 255 | 241 | 0.1905 | HOMO → LUMO+1 HOMO-1 → LUMO |
| 328 | 343 | 0.5802 | HOMO → LUMO |

was not considered in the theoretical calculation. Figure 4 shows counter plots and the energy of some selected FMOs active in the electronic transitions. Based on the B3LYP/6-311G optimized geometry, the natural population analysis indicates that the occupied and unoccupied orbitals were mainly composed of *p* atomic orbitals. As shown in Fig. 4 and Table 6, the electrons are transferred between the two phenyl ring and pyrazolone ring, which corresponds to the $n \rightarrow \pi^*$ and $\pi \rightarrow \pi^*$ electronic transition.

Fluorescence Spectra

The fluorescence spectrum was measured in an ethanol solution to determine the fluorescence property of the title compound (Fig. 6). A maximum emission band at 370 nm was observed in the spectrum, indicating that the title compound has no potential fluorescence property.

Antioxidant Activity

The DPPH antioxidant assay was performed using the Blois method and the results are presented in Table 7.

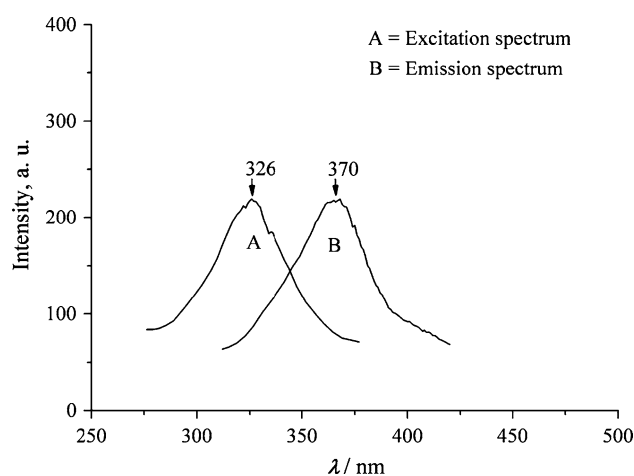
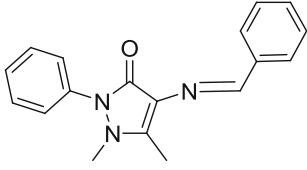
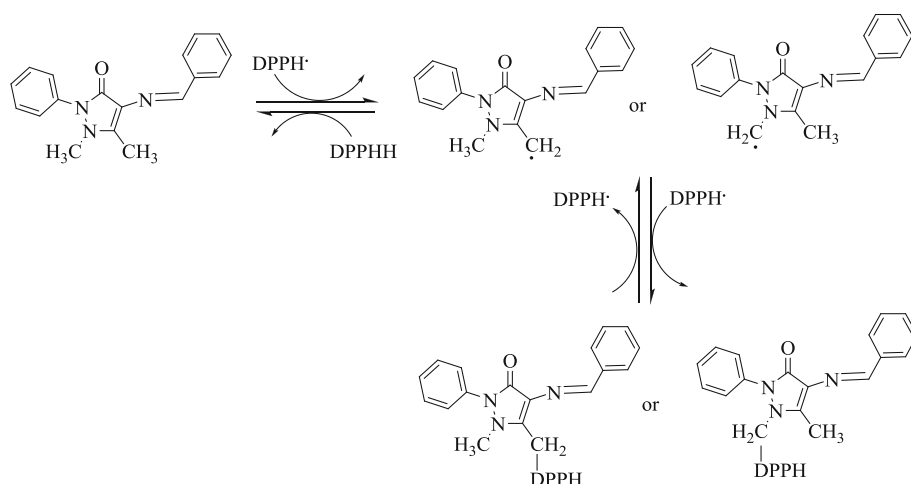


Fig. 6 Fluorescence spectra of the title compound

Table 7 Free radical scavenging activity of title compound observed with DPPH assay

| Sample | Conc. (mg/ml) | % Inhibition | IC ₅₀ (μM) |
|--|---------------|--------------|-----------------------|
|  Ascorbic acid | 20 | 92.78 | 31.26 |
| | 15 | 85.45 | |
| | 10 | 53.65 | |
| | 5 | 28.22 | |
| | 2.5 | 15.56 | |
| | 0.25 | 96.52 | |
| | 0.125 | 96.52 | |
| | 0.0625 | 49 | |
| | 0.0312 | 29.6 | |
| | 0.0156 | 12.4 | |

The title compound displayed strong antioxidant activity with an IC₅₀ value of 31.26 μM. Ascorbic acid, a phenolic antioxidant has been used as a positive control which showed stronger antioxidant activity (IC₅₀ value of 0.41 μM) than that of the title compound. The mechanism of phenolic antioxidants is well known. However, there has been an increase in interest in understanding and characterizing the mechanism of non phenolic antioxidants. Thus, it would be interesting to examine the relationship between the electrochemical properties and molecular structures of antioxidants. Table 5 shows that a high electron density was located near the –N1–N2– (–0.610, –0.400) and –C9–N3– (–0.203, –0.358) bonds. This finding implies that these atom groups may be subject to oxidation. The carbons of two methyl groups, C11 (–0.584) and –C7– (–0.394) also bear a high electron density and may produce proton free radicals to neutralize the DPPH (Fig. 7). However, the radical formed from the title compounds was not sufficiently stabilized through resonance; thus, many

Fig. 7 Proposed mechanism for the DPPH[•] reaction

different reactions are possible. To support our proposed reaction mechanism, it would be interesting to characterize the reaction products using liquid chromatograph coupled with a mass spectrometer.

Conclusions

In this study, we synthesized a single crystal of a Schiff base ligand of 4-amino-1,5-dimethyl-2-phenylpyrazole-3-one using a condensation reaction with benzaldehyde. X-ray diffraction analysis reveals that the structure of (*E*)-4-[benzylideneamino]-1,5-dimethyl-2-phenyl-1*H*-pyrazol-3(2*H*)-one had monoclinic (*P*2₁/*c*) symmetry and a *trans* configuration around the central C=N double bond. The unit cell of the molecular packing was composed of four molecules and formed inversion related dimmers. The optimized geometries and electronic structures of the title compound using B3LYP/6-311G calculations revealed a close relation with the crystal structure. The comparison between the experimental and predicted data indicates that the 6-311G basis set at a density functional B3LYP level can be used to accurately predict the vibrational frequencies. UV–Vis absorption spectra were simulated using TD-DFT calculations. The NBO analyses suggest that the electronic spectra were mainly due to the $n \rightarrow \pi^*$ and $\pi \rightarrow \pi^*$ electronic transition. The DPPH antioxidant activity of the title compound might be due to the formation of proton free radicals by the C7 or C11 methyl groups.

Supplementary Material

Crystallographic data for the structure of the title compound have been deposited in the Cambridge Crystallographic Data Center (Deposition number CCDC-783980). The data can be obtained, free of charge, upon request

from: Cambridge Crystallographic Data Center (CCDC), 12 Union Road, Cambridge CB2 1EZ, UK; fax: +44(0) 1222-336033; e-mail: deposit@ccdc.cam.ac.uk; www.ccdc.cam.ac.uk/data_request/cif.

References

1. Ali MA, Mirza AH, Butcher RJ, Tarafder MTH, Keat TB, Ali AM (2002) J Inorg Biochem 92:141–148
2. Cukurovali A, Yilmaz I, Ozmen H, Ahmedzade M (2002) Transit Met Chem 27:171–176
3. Santos MLP, Bagatin IA, Pereira EM, Ferreira AMDC (2001) J Chem Soc Dalton Trans 838–844
4. Ismail KZ (2000) Transit Met Chem 25:522–528
5. Abd Rehim SS, Ibrahim MAM, Khalid KF (2001) Mater Chem Phys 70:268–273
6. Yadav PN, Demertzis MA, Kovala-Demertzi D, Skoulika S, West DX (2003) Inorg Chim Acta 349:30–36
7. Forest SE, Stimson MJ, Simon JD (1999) J Phys Chem B103: 3963–3965
8. Nazeeruddin MK, Angelis FD, Fantacci S, Selloni A, Viscardi G, Liska P, Ito S, Takeru B, Grätzel M (2005) J Am Chem Soc 127:16835–16847
9. Xu J, Zhang H, Wang L, Liang G, Wang L, Shen X, Xu W (2010) Monatsh Chem 141:549–555
10. Lee C, Sohlberg K (2010) Chem Phys 367:7–19
11. Ji N-N, Shi Z-Q, Zhao R-G, Zheng Z-B, Li Z-F (2010) Bull Korean Chem Soc 31:881–886
12. Zhao W-N (2007) Acta Crystallogr E63:m2095
13. Montalvo-González R, Ariza-Castolo A (2003) J Mol Struct 655:375–389
14. Li Z-X, Zhang X-L (2006) Chin J Struct Chem 25:29–32
15. Hu T-P (2006) Acta Crystallogr E62:o2270–o2271
16. Zhang Q-Z, Zhao Y-L, Chen X, Yu M (2006) Acta Crystallogr E62:o5252–o5254
17. Liu S-X, Han J-R, Zhen X-L, Tian X (2006) Acta Crystallogr E62:o5765–o5766
18. Bruker (2000) SMART (version 5.625) for Windows NT. Bruker AXS Inc., Madison
19. Sheldrick GM (2008) Acta Crystallogr A64:112–122
20. Sheldrick GM (2008) SHELXTL. Version 6.12 for Windows NT. Bruker AXS Inc., Madison

21. Bruker (2000) SAINT (version 5.625) for Windows NT. Bruker AXS Inc., Madison
22. Dewar MJS, Zoebisch EG, Healy EF (1985) *J Am Chem Soc* 107:3902–3909
23. Becke AD (1993) *J Chem Phys* 98:5648–5652
24. Lee C, Yang W, Parr RG (1988) *Phys Rev B* 37:785–789
25. Schmidt MW, Baldrige KK, Boatz JA, Elbert ST, Gordon MS, Jensen JH, Koseki S, Matsunaga N, Nguyen KA, Su S, Windus TL, Dupuis M, Montgomery JA Jr (1993) *J Comput Chem* 14:1347–1363
26. Blois MS (1958) *Nature* 181:1199–1200
27. Allen FH, Kennard O, Watson DG, Brammer L, Orpen AG, Taylor R (1987) *J Chem Soc Perkin Trans II* S1–S19
28. Zhao PS, Shao DL, Zhang J, Wei Y, Jian FF (2009) *Bull Korean Chem Soc* 30:1667–1670
29. Jian FF, Zhao PS, Yu Q, Wang QX, Jiao K (2004) *J Phys Chem A* 108:5258–5267
30. Xia SW, Xu X, Sun YL, Fan YH, Bi CF, Zhang DM, Yang LR (2006) *Chin J Struct Chem* 25:197–203
31. Mendizabal F, Olea-Azar C (2005) *Int J Quant Chem* 103:34–44